Centralized Path Planning for Unmanned Aerial Vehicles with A Heterogeneous Mix of Sensors

Kutluyıl Doğançay [#1], Hatem Hmam [*2], Samuel P. Drake [*3], Anthony Finn [*4]

[#] *School of Electrical and Information Engineering, University of South Australia*
Mawson Lakes, SA 5095, Australia
[1] k.dogancay@ieee.org

[*] *Electronic Warfare and Radar Division, Defence Science and Technology Organisation*
Edinburgh, SA 5111, Australia
[2] Hatem.Hmam@dsto.defence.gov.au
[3] Sam.Drake@dsto.defence.gov.au
[4] Anthony.Finn@dsto.defence.gov.au

***Abstract*—This paper is concerned with real-time optimal UAV path planning in a multi-emitter geolocation environment. All UAVs are assumed to be controlled by a central processing unit. A UAV waypoint-update/steering algorithm is developed based on maximizing the determinant of Fisher information matrix for localization of stationary emitters. Soft and hard geometric constraints for threat/collision avoidance are also implemented. An effective joint path optimization and dynamic sensor allocation algorithm is proposed to handle communication bandwidth constraints. The performance of the developed steering algorithm is illustrated with extensive simulation examples.**

I. Introduction

Passive geolocation of RF emitters using multiple observers has been an active research area (see e.g. [1], [2], [3], [4] and the references therein). In this paper we consider the geolocation of multiple emitters using several unmanned aerial vehicles (UAVs) equipped with a heterogeneous mix of sensors. In multi-emitter geolocation problems individual UAVs are assigned to teams based on a pre-mission plan that uses any prior knowledge available, such as coarse estimates of emitter locations and any geometric constraints. For UAVs with time-difference-of-arrival sensors teaming algorithms have been proposed in [5]. Teaming and path planning are carried out concurrently since they are both affected by dynamic changes in the environment. In emitter localization the key objective is to locate emitters with high accuracy. Path optimization must therefore achieve improved localization performance using a well-defined performance indicator.

We minimize the area of error ellipse or estimation uncertainty as the path optimization criterion, which is equivalent to maximizing the determinant of Fisher information matrix [6]. In the context of optimal experimental design it is also known as the *D-optimality criterion* [7], [8], [9]. This approach has been successfully applied to online path optimization for UAVs equipped with scan-based sensors [10].

In this paper we focus on centralized UAV path planning which implies that all UAVs are controlled by a central processing unit (this is essential for inter-team collision avoidance). The UAVs are allowed to have different payload sensors for passive localization. We develop UAV steering algorithms to optimize the geolocation performance based on maximization of the determinant of Fisher information matrix. The proposed steering algorithm is also capable of implementing soft geometric constraints for threat or obstacle avoidance, as well as, collision avoidance. In addition, hard constraints around estimated emitter locations are established in order to maintain a certain minimum distance from the emitters mainly for signal reception purposes. A myopic joint path optimization and dynamic sensor allocation technique is developed to meet communication bandwidth constraints.

The paper is organized as follows. Section II states the path planning problem and develops the UAV steering algorithm based on maximizing the determinant of Fisher information matrix. In Section III the implementation of hard and soft geometric constraints is discussed. Section IV proposes a simple and effective joint path optimization and dynamic sensor allocation technique. In Section V we derive the hybrid maximum likelihood estimator for emitter location. Section VI presents simulation studies and the paper concludes in Section VII.

II. Centralized Gradient Based Path Optimization

A. Problem Definition

We consider 2D localization of stationary emitters. The UAVs are assigned to N teams each with K_i UAVs, $i = 1, \ldots, N$. The total number of UAVs is $K_1 + K_2 + \cdots + K_N$. UAV team i is tasked to geolocate an emitter at unknown location $\boldsymbol{s}_i$. The waypoints for UAVs are updated at discrete time instants $k = 1, 2, \ldots$. The waypoint updates and sensor measurements are assumed to be synchronized in time. Strictly speaking this assumption is not necessary. However it simplifies the development of algorithms. The UAVs are allowed to carry multiple sensors. The possible sensors are scan-based (SC), angle-of-arrival (AOA) and time-difference-of-arrival (TDOA) sensors. The sensor measurement errors are assumed to be zero-mean Gaussian. Even though a UAV can have multiple sensors, only one sensor is assumed to operate at measurement time instants due to limited communication bandwith from UAVs to the central processing unit. The UAVs

are equipped with GPS so that the central processing unit can query their locations. At time instant k, the location of UAV j in team i is denoted by $\boldsymbol{p}_{ij}(k)$, $i = 1, \ldots, N$, $j = 1, \ldots, K_i$.

The minimum number of UAVs in a team depends on the sensors used. For example, if all UAVs are equipped with AOA sensors, a minimum of two UAVs is required to localize an emitter. For scan-based and TDOA sensors the minimum number of UAVs is three. Note that SC and TDOA measurements require at least a pair of UAVs.

The central processing unit steers UAVs by generating waypoints upon receiving sensor measurements and current UAV positions. The UAV waypoint update algorithm is given by the iteration

$$\boldsymbol{p}_{ij}(k+1) = \boldsymbol{p}_{ij}(k) + \boldsymbol{u}_{ij}(k), \quad i = 1, \ldots, N, \quad j = 1, \ldots, K_i, \quad k = 0, 1, \ldots. \tag{1}$$

The waypoint update vector $\boldsymbol{u}_{ij}(k)$ satisfies the norm constraint $\|\boldsymbol{u}_{ij}(k)\| = vT$ where v is the cruising speed of UAVs (assumed to be the same for all UAVs with no loss of generality) and T is the time interval between waypoint updates. The angle of $\boldsymbol{u}_{ij}(k)$ is constrained by the turn rate of the UAVs φ (rad/s). In what follows we develop centralized path planning algorithms to generate waypoint updates $\boldsymbol{u}_{ij}(k)$ that maximize the localization performance while avoiding geometric constraints.

B. Estimation Uncertainty Minimization

Suppose that the emitter location estimator in use is unbiased and efficient, i.e., its covariance matrix is identical to the Cramer-Rao lower bound (CRLB). Then the area of the 1-σ error ellipse (39.4% confidence region) of the location estimate is given by

$$A_{1\sigma} = \frac{\pi}{|\boldsymbol{\Phi}(\boldsymbol{s}_i)|^{1/2}}. \tag{2}$$

where $\boldsymbol{\Phi}(\boldsymbol{s}_i)$ is the Fisher information matrix and $|\cdot|$ denotes determinant [6]. In other words, the estimation uncertainty area is inversely proportional to the determinant of the Fisher information matrix. Therefore maximizing the determinant of the Fisher information matrix is equivalent to minimizing the estimation uncertainty area, which means improved localization performance. Whilst (2) is valid for efficient estimators, it can also be used for a maximum likelihood estimator if measurement noise levels justify approximate efficiency.

A UAV steering algorithm can be developed by adopting a gradient based approach where the objective function to be maximized over UAV locations is given by the determinant of an approximation of $\boldsymbol{\Phi}(\boldsymbol{s}_i)$:

$$J(\boldsymbol{\pi}_i(k)) = |\boldsymbol{\Phi}(\hat{\boldsymbol{s}}_i(k))| \tag{3}$$

where $\hat{\boldsymbol{s}}_i(k)$ is the maximum likelihood estimate of $\boldsymbol{s}_i$ at time k and $\boldsymbol{\pi}_i(k)$ is the vector of UAV locations in team i at time k:

$$\boldsymbol{\pi}_i(k) = \begin{bmatrix} \boldsymbol{p}_{i1}(k) \\ \vdots \\ \boldsymbol{p}_{i,K_i}(k) \end{bmatrix}. \tag{4}$$

Maximizing $J(\boldsymbol{\pi}_i(k))$ over UAV locations at waypoint updates leads to the gradient based steering algorithm:

$$\boldsymbol{\pi}_i(k+1) = \boldsymbol{\pi}_i(k) + \boldsymbol{M}_i(k)\frac{\partial J(\boldsymbol{\pi}_i(k))}{\partial \boldsymbol{\pi}_i(k)}, \quad k = 0, 1, \ldots \tag{5}$$

where $\boldsymbol{M}_i(k)$ is a time-varying matrix that normalizes the gradient of $J(\boldsymbol{\pi}_i(k))$:

$$\boldsymbol{M}_i(k) = \begin{bmatrix} \mu_{i1}\boldsymbol{I}_2 & & \boldsymbol{0} \\ & \ddots & \\ \boldsymbol{0} & & \mu_{iK_i}\boldsymbol{I}_2 \end{bmatrix}, \qquad \mu_{ij} = \frac{vT}{\|\partial J(\boldsymbol{\pi}_i(k))/\partial \boldsymbol{p}_{ij}(k)\|} \tag{6}$$

and $\boldsymbol{I}_2$ is the 2×2 identity matrix. The normalization matrix ensures that the UAVs cruise at a constant speed. This is particularly important for small UAVs, such as the Aerosonde UAV, with small air speed envelopes. The use of $\boldsymbol{M}(k)$ makes the waypoint updates insensitive to scaling of the Fisher information matrix. This implies that any unknown proportionality constant present in the Fisher information matrix can be ignored. If the waypoint update vectors obtained from (5) violate the maximum turn rate φ, they must be re-calculated using the maximum turn rate.

Rather than derive analytical expressions for the gradient of $J(\boldsymbol{\pi}_i(k))$ in (5) we opt for numerical computation based on the first-order finite difference approximation:

$$\frac{\partial J(\boldsymbol{\pi}_i(k))}{\partial \pi_l(k)} \approx \frac{J(\boldsymbol{\pi}_i(k) + \boldsymbol{\Delta}_l) - J(\boldsymbol{\pi}_i(k))}{\Delta} \tag{7}$$

where $\pi_l(k)$ is the lth entry of $\boldsymbol{\pi}_i(k)$, $l = 1, \ldots, 2K_i$, and $\boldsymbol{\Delta}_l$ is a $2K_i \times 1$ column vector with zero entries except for the lth entry which is equal to Δ. Here Δ is a small positive real number (interval parameter). The accuracy of the approximation increases as Δ is decreased.

The objective function $J(\boldsymbol{\pi}_i(k))$ does not always produce the fastest reduction in the mean-square error (MSE) for emitter location estimate because the iterative steering algorithm (5) is only locally optimal and does not exploit the global topology of the objective function. In certain situations this may result in favouring baseline expansion for the UAVs instead of heading for the emitter. The UAVs should be attracted towards the emitter in addition to maximizing the determinant of the Fisher information matrix as it tends to infinity when all UAVs are at the true emitter location. One way to trade baseline expansion for range reduction is to use the following modified cost function [10]

$$J'(\boldsymbol{\pi}_i(k)) = \frac{J(\boldsymbol{\pi}_i(k))}{\sum_{j=1}^{K_i} \left\|\boldsymbol{p}_{ij}(k) - \hat{\boldsymbol{s}}_i(k)\right\|^{\beta_i}} \tag{8}$$

where $\beta_i \geq 0$ is the force parameter that determines the sensitivity of the objective function to emitter range reduction. The normalization term introduced into $J'(\cdot)$ provides a tradeoff between baseline expansion and range minimization. When $\beta_i = 0$, $J'(\cdot)$ and $J(\cdot)$ produce identical trajectories. Small β_i provides good initial geolocation performance and

slow convergence. As β_i increases, the UAVs are steered towards the emitter with greater force. This results in faster UAV convergence to the emitter at the expense of some initial performance loss if the UAVs did not have a sufficiently large baseline [10].

C. UAV Teams with Heterogeneous Sensors

When UAVs in a team have different sensors emitter geolocation is performed using a hybrid estimator. The Fisher information matrix for a hybrid estimator employing AOA, TDOA and SC sensors is given by

$$\begin{aligned}\boldsymbol{\Phi}_{\mathrm{H}}(\boldsymbol{s}_i) &= \boldsymbol{J}_{\mathrm{A}}^T(\boldsymbol{s}_i)\boldsymbol{\Sigma}_{\mathrm{A}}^{-1}(\boldsymbol{s}_i)\boldsymbol{J}_{\mathrm{A}}(\boldsymbol{s}_i) \\ &+ \boldsymbol{J}_{\mathrm{TD}}^T(\boldsymbol{s}_i)\boldsymbol{\Sigma}_{\mathrm{TD}}^{-1}(\boldsymbol{s}_i)\boldsymbol{J}_{\mathrm{TD}}(\boldsymbol{s}_i) + \boldsymbol{J}_{\mathrm{S}}^T(\boldsymbol{s}_i)\boldsymbol{\Sigma}_{\mathrm{S}}^{-1}(\boldsymbol{s}_i)\boldsymbol{J}_{\mathrm{S}}(\boldsymbol{s}_i) \quad (9)\end{aligned}$$

where $\boldsymbol{J}_{\mathrm{X}}(\boldsymbol{s}_i)$ is the Jacobian of the measurement error for UAVs carrying sensor X in team i (here X is A for AOA sensors, TD for TDOA sensors, and S for SC sensors) and $\boldsymbol{\Sigma}_{\mathrm{X}}(\boldsymbol{s}_i)$ is the measurement error covariance matrix. For UAV teams with heterogeneous sensors the objective function in (3) becomes

$$J(\boldsymbol{\pi}_i(k)) = |\boldsymbol{\Phi}_{\mathrm{H}}(\hat{\boldsymbol{s}}_i(k))| \quad (10)$$

where $\hat{\boldsymbol{s}}_i(k)$ is now the maximum likelihood hybrid estimate of the emitter location (see Section V). Let $\boldsymbol{p}_{ij}^{\mathrm{X}}(k)$, $i = 1, \ldots, N$, $j = 0, \ldots, K_{\mathrm{X}}(i)$ denote the locations of UAVs at time k that carry sensor X in team i. Here $K_{\mathrm{A}}(i)+K_{\mathrm{TD}}(i)+K_{\mathrm{S}}(i) = K_i$.

At time k the Jacobian and covariance matrix for UAVs with AOA sensors are

$$\boldsymbol{J}_{\mathrm{A}}(\boldsymbol{s}_i) = \begin{bmatrix} \frac{[\sin\theta_1(\boldsymbol{s}_i), -\cos\theta_1(\boldsymbol{s}_i)]}{\|\boldsymbol{s}_i - \boldsymbol{p}_{i1}^{\mathrm{A}}(k)\|} \\ \vdots \\ \frac{[\sin\theta_{K_{\mathrm{A}}(i)}(\boldsymbol{s}_i), -\cos\theta_{K_{\mathrm{A}}(i)}(\boldsymbol{s}_i)]}{\|\boldsymbol{s}_i - \boldsymbol{p}_{i,K_{\mathrm{A}}(i)}^{\mathrm{A}}(k)\|} \end{bmatrix}_{K_{\mathrm{A}}(i)\times 2},$$

$$\theta_j(\boldsymbol{s}_i) = \angle(\boldsymbol{s}_i - \boldsymbol{p}_{ij}^{\mathrm{A}}(k)) \quad (11)$$

and

$$\boldsymbol{\Sigma}_{\mathrm{A}}(\boldsymbol{s}_i) = \sigma_{\mathrm{A}}^2 \begin{bmatrix} \|\boldsymbol{d}_{i1}^{\mathrm{A}}(k)\|^\gamma & & \boldsymbol{0} \\ & \ddots & \\ \boldsymbol{0} & & \|\boldsymbol{d}_{i,K_{\mathrm{A}}(i)}^{\mathrm{A}}(k)\|^\gamma \end{bmatrix} \quad (12)$$

where σ_{A}^2 is the AOA noise variance at unit range, $0 \le \gamma < 2$ is the power loss exponent, $\angle\boldsymbol{z}$ denotes the bearing angle vector $\boldsymbol{z}$ makes with the positive x-axis, and

$$\boldsymbol{d}_{ij}^{\mathrm{X}}(k) = \boldsymbol{s}_i - \boldsymbol{p}_{ij}^{\mathrm{X}}(k). \quad (13)$$

The sensor measurement noise variances get larger with increasing emitter range.

For TDOA sensors the Jacobian and covariance matrix are given by

$$\boldsymbol{J}_{\mathrm{TD}}(\boldsymbol{s}_i) = \begin{bmatrix} \frac{(\boldsymbol{s}_i - \boldsymbol{p}_{i2}^{\mathrm{TD}}(k))^T}{\|\boldsymbol{d}_{i2}^{\mathrm{TD}}(k)\|} - \frac{(\boldsymbol{s}_i - \boldsymbol{p}_{i1}^{\mathrm{TD}}(k))^T}{\|\boldsymbol{d}_{i1}^{\mathrm{TD}}(k)\|} \\ \vdots \\ \frac{(\boldsymbol{s}_i - \boldsymbol{p}_{i,K_{\mathrm{TD}}(i)}^{\mathrm{TD}}(k))^T}{\|\boldsymbol{d}_{i,K_{\mathrm{TD}}(i)}^{\mathrm{TD}}(k)\|} - \frac{(\boldsymbol{s}_i - \boldsymbol{p}_{i1}^{\mathrm{TD}}(k))^T}{\|\boldsymbol{d}_{i1}^{\mathrm{TD}}(k)\|} \end{bmatrix}_{(K_{\mathrm{TD}}(i)-1)\times 2} \quad (14)$$

and

$$\boldsymbol{\Sigma}_{\mathrm{TD}}(\boldsymbol{s}_i) = \sigma_{\mathrm{TD}}^2 \left(\|\boldsymbol{d}_{i1}^{\mathrm{TD}}(k)\|^\gamma \begin{bmatrix} 1 & \cdots & 1 \\ \vdots & \ddots & \vdots \\ 1 & \cdots & 1 \end{bmatrix} + \begin{bmatrix} \|\boldsymbol{d}_{i2}^{\mathrm{TD}}(k)\|^\gamma & & \boldsymbol{0} \\ & \ddots & \\ \boldsymbol{0} & & \|\boldsymbol{d}_{i,K_{\mathrm{TD}}(i)}^{\mathrm{TD}}(k)\|^\gamma \end{bmatrix} \right) \quad (15)$$

where σ_{TD}^2 is the TDOA noise variance at unit range. The TDOA localization algorithm assumes that $\boldsymbol{p}_{i1}^{\mathrm{TD}}(k)$ is the reference receiver; i.e., time differences are measured with respect to the sensor at $\boldsymbol{p}_{i1}^{\mathrm{TD}}(k)$.

The Jacobian for SC sensors is

$$\boldsymbol{J}_{\mathrm{S}}(\boldsymbol{s}_i) = \frac{\partial \boldsymbol{e}_{\mathrm{S}}(\boldsymbol{s}_i)}{\partial \boldsymbol{s}_i} \quad (16)$$

where $\boldsymbol{e}_{\mathrm{S}}(\boldsymbol{s}_i) = [e_{12}, e_{23}, \ldots, e_{K_{\mathrm{S}}(i)-1,K_{\mathrm{S}}(i)}]^T$ is the SC error vector. The entries of the Jacobian are given by

$$\begin{aligned}\frac{\partial e_{mn}}{\partial \boldsymbol{s}_i} &= -\frac{\partial}{\partial \boldsymbol{s}_i}\cos^{-1} h_{mn} && (17a)\\ &= \frac{1}{\delta_{mn}\sqrt{1-h_{mn}^2}}\Bigg(\boldsymbol{d}_{im}^{\mathrm{S}}(k) + \boldsymbol{d}_{in}^{\mathrm{S}}(k) && (17b)\\ &\quad - \eta_{mn}\left(\frac{\boldsymbol{d}_{im}^{\mathrm{S}}(k)}{\|\boldsymbol{d}_{im}^{\mathrm{S}}(k)\|_2^2} + \frac{\boldsymbol{d}_{in}^{\mathrm{S}}(k)}{\|\boldsymbol{d}_{in}^{\mathrm{S}}(k)\|_2^2}\right)\Bigg) && (17c)\end{aligned}$$

where

$$h_{mn} = \frac{\eta_{mn}}{\delta_{mn}}, \quad \eta_{mn} = \left(\boldsymbol{d}_{im}^{\mathrm{S}}(k)\right)^T \boldsymbol{d}_{in}^{\mathrm{S}}(k),$$
$$\delta_{mn} = \|\boldsymbol{d}_{im}^{\mathrm{S}}(k)\|\|\boldsymbol{d}_{in}^{\mathrm{S}}(k)\|.$$

The covariance matrix of SC sensor errors is

$$\boldsymbol{\Sigma}_{\mathrm{S}}(\boldsymbol{s}_i) = \omega^2\sigma_{\mathrm{S}}^2 \begin{bmatrix} \varsigma_{12} & -\varsigma_2 & & & \boldsymbol{0} \\ -\varsigma_2 & \varsigma_{23} & -\varsigma_3 & & \\ & -\varsigma_3 & \varsigma_{34} & \ddots & \\ & & \ddots & \ddots & -\varsigma_{K_{\mathrm{S}}(i)-1} \\ \boldsymbol{0} & & & -\varsigma_{K_{\mathrm{S}}(i)-1} & \varsigma_{K_{\mathrm{S}}(i)-1,K_{\mathrm{S}}(i)} \end{bmatrix} \quad (18)$$

where ω is the scan rate for the emitter, σ_{S}^2 is the SC sensor noise variance at unit range, and

$$\varsigma_{mn} = \|\boldsymbol{d}_{im}^{\mathrm{S}}(k)\|^\gamma + \|\boldsymbol{d}_{in}^{\mathrm{S}}(k)\|^\gamma$$
$$\varsigma_m = \|\boldsymbol{d}_{im}^{\mathrm{S}}(k)\|^\gamma.$$

III. Geometric Constraints

In this section we introduce hard and soft constraints to realize threat/collision avoidance. Soft constraints can be thought of as desirable behaviours for which failure to adhere to is penalized by decreasing the objective function. Hard constraints are those which cannot be violated.

A different terminology is used to describe constraints in the classical mechanics literature [11]. In classical mechanics soft constraints are embedded in the Lagrangian and are not referred to as constraints at all. Hard constraints are divided

into two types, holonomic and nonholonomic. Holonomic constraints are those which can be defined in terms of an equality function, e.g., $f(\boldsymbol{p}_{ij}(k)) = 0$ for all k. Non-holonomic constraints on the other hand are defined in terms of an inequality, e.g. $f(\boldsymbol{p}_{ij}(k)) \leq 0$ for all k. An example of a holonomic constraint is if a UAV was required to be a certain distance from an emitter. An example of a nonholonomic constraint is if a UAV cannot get too close to a pop-up threat.

A. Soft Constraints (Modification of the Objective Function)

Collision avoidance and avoidance of threats and obstacles is achieved by modifying the object function $J'(\boldsymbol{\pi}_i(k))$ so that

$$J_{\mathrm{C}}(\boldsymbol{\pi}_i(k)) = J'(\boldsymbol{\pi}_i(k)) \underbrace{\prod_{j=1}^{K_i}\prod_{l=1}^{N_T}\left(1-e^{-\|\boldsymbol{p}_{ij}(k)-\boldsymbol{c}_l\|/\kappa_l}\right)}_{\text{threat avoidance}} \times \underbrace{\prod_{m>j}^{K_i}\left(1-e^{-\|\boldsymbol{p}_{ij}(k)-\boldsymbol{p}_{im}(k)\|/\rho}\right)}_{\text{intra-team collision avoidance}} \times \underbrace{\prod_{\substack{n=1\\n\neq i}}^{N}\prod_{q=1}^{K_n}\left(1-e^{-\|\boldsymbol{p}_{ij}(k)-\boldsymbol{p}_{nq}(k)\|/\rho}\right)}_{\text{inter-team collision avoidance}} \quad (19)$$

where N_T is the number of threats, the $\boldsymbol{c}_l$ are the estimated threat locations, the $\kappa_l > 0$ are the threat avoidance parameters, and $\rho > 0$ is the clearance parameter for collision avoidance. The factors introduced to $J_C(\boldsymbol{\pi}_i(k))$ create global unstable minima at threat and collision locations. This ensures that the gradient based UAV steering algorithm avoids these unstable locations as desired.

B. Hard Constraints (Nonholonomic Constraints)

Due to the vertical beamwidth of radars a UAV must be greater than a certain distance d_i from a radar located at $\boldsymbol{s}_i$. We consider this a hard constraint because a UAV inside this distance will not be able to detect the radar and hence will be ineffective. If the jth UAV in team i reaches a distance d_i from emitter i, the hard constraint projects it onto a circle of radius d_i centred at the estimated emitter location:

$$\boldsymbol{p}_{ij}(k+1) = d_i \frac{\boldsymbol{p}_{ij}(k+1) - \hat{\boldsymbol{s}}_i(k)}{\|\boldsymbol{p}_{ij}(k+1) - \hat{\boldsymbol{s}}_i(k)\|} + \hat{\boldsymbol{s}}_i(k). \quad (20)$$

This projection is motivated by the dependence of optimal location performance on angular separation when all sensors are equidistant from the emitter. Indeed, when all UAVs reach the hard constraint, they eventually attain the optimal angular separation minimizing the MSE.

The waypoint projection in (20) can easily violate the maximum turn rate φ and the update norm constraint $\|\boldsymbol{u}_{ij}(k)\| = vT$. To remedy this we use a larger d_i than what is required to allow circular loop flights into the hard constraint, and replace projected waypoint updates with control vectors that are compliant with the turn rate and the update norm.

IV. Joint Path Planning and Dynamic Sensor Allocation

Suppose that each UAV is equipped with an SC, AOA and TDOA sensor. Given the bandwidth bottleneck for transmitting data from UAVs to the central processing unit, it may be possible to transmit only one sensor's data from each UAV. The question then arises as to which sensor out of SC, AOA and TDOA should be selected at each waypoint update in order to provide the best localization performance. The resulting sensor allocation also affects the UAV paths because of changes to the Fisher information matrix $\boldsymbol{\Phi}_{\mathrm{H}}(\boldsymbol{s}_i)$. This leads to a joint path optimization and dynamic sensor allocation problem.

We develop a myopic dynamic sensor allocation algorithm attempting to maximize the objective function at each waypoint update without consideration of long-term effects. For the sake of simplicity we consider UAV teams with three UAVs, i.e., $K_i = 3$, $i = 1, \ldots, N$. The permissible sensor combinations for each UAV team are listed in Table I.

TABLE I
Permissible Sensor Combinations

$\mathcal{C}$	UAV 1	UAV 2	UAV 3
1	SC	SC	SC
2	AOA	AOA	AOA
3	TDOA	TDOA	TDOA
4	SC	SC	AOA
5	SC	AOA	SC
6	AOA	SC	SC
7	TDOA	TDOA	AOA
8	TDOA	AOA	TDOA
9	AOA	TDOA	TDOA

The sensor combination to be used is determined from

$$\mathcal{C}^*(k+1) = \underset{1\leq\mathcal{C}\leq 9}{\arg\max} \, |\boldsymbol{\Phi}_{\mathrm{H}}(\hat{\boldsymbol{s}}_i(k), \mathcal{C})| \quad (21)$$

where $\mathcal{C}^*(k+1)$ is the sensor allocation at time instant $k+1$, and $\boldsymbol{\Phi}_{\mathrm{H}}(\hat{\boldsymbol{s}}_i(k), \mathcal{C})$ makes explicit the dependence of the Fisher information matrix on sensor allocation (see (9)).

Dynamic sensor allocation will make an impact on optimal path planning in the case of comparable sensor performances. If a subset of sensors have much lower noise variances than others, they will tend to dominate sensor allocation decisions despite dynamic changes in the localization geometry.

V. Maximum Likelihood Estimator

In this section we present the details of the hybrid maximum likelihood estimator (MLE) to be used in conjunction with the path planning algorithm. The maximum likelihood cost function for hybrid localization by UAV team i, $i = 1, \ldots, N$, is given by

$$J_{\mathrm{MLE}}(\boldsymbol{s}_i) = \underbrace{J_{\mathrm{S}}(\boldsymbol{s}_i)}_{\text{scan-based}} + \underbrace{J_{\mathrm{A}}(\boldsymbol{s}_i)}_{\text{AOA}} + \underbrace{J_{\mathrm{TD}}(\boldsymbol{s}_i)}_{\text{TDOA}}. \quad (22)$$

Here $J_{\mathrm{S}}(\boldsymbol{s}_i)$ is the scan-based cost function:

$$J_{\mathrm{S}}(\boldsymbol{s}_i) = \boldsymbol{e}_{\mathrm{S}}^T(\boldsymbol{s}_i)\boldsymbol{\Sigma}_{\mathrm{S}}^{-1}(i)\boldsymbol{e}_{\mathrm{S}}(\boldsymbol{s}_i), \quad \boldsymbol{e}_{\mathrm{S}}(\boldsymbol{s}_i) = \hat{\boldsymbol{\alpha}}(\boldsymbol{s}_i) - \boldsymbol{\alpha}(\boldsymbol{s}_i)$$

where $\hat{\boldsymbol{\alpha}}(\boldsymbol{s}_i)$ is the vector of subtended angle measurements for emitter i and $\boldsymbol{\alpha}(\boldsymbol{s}_i)$ contains exact subtended angles as a function of emitter location $\boldsymbol{s}_i$:

$$\hat{\boldsymbol{\alpha}}(\boldsymbol{s}_i) = \begin{bmatrix} \hat{\alpha}_{12}(\boldsymbol{s}_i) \\ \vdots \\ \hat{\alpha}_{K_{\rm S}(i)-1,K_{\rm S}(i)}(\boldsymbol{s}_i) \end{bmatrix}$$

$$\boldsymbol{\alpha}(\boldsymbol{s}_i) = \begin{bmatrix} \cos^{-1}\frac{\left(\boldsymbol{d}^{\rm S}_{i1}\right)^T \boldsymbol{d}^{\rm S}_{i2}}{\|\boldsymbol{d}^{\rm S}_{i1}\|\|\boldsymbol{d}^{\rm S}_{i2}\|} \\ \vdots \\ \cos^{-1}\frac{\left(\boldsymbol{d}^{\rm S}_{i,K_{\rm S}(i)-1}\right)^T \boldsymbol{d}^{\rm S}_{i,K_{\rm S}(i)}}{\|\boldsymbol{d}^{\rm S}_{i,K_{\rm S}(i)-1}\|\|\boldsymbol{p}^{\rm S}_{i,K_{\rm S}(i)}\|} \end{bmatrix}.$$

The AOA cost function is

$$J_{\rm A}(\boldsymbol{s}_i) = \boldsymbol{e}_{\rm A}^T(\boldsymbol{s}_i)\boldsymbol{\Sigma}_{\rm A}^{-1}(i)\boldsymbol{e}_{\rm A}(\boldsymbol{s}_i), \quad \boldsymbol{e}_{\rm A}(\boldsymbol{s}_i) = \hat{\boldsymbol{\theta}}(\boldsymbol{s}_i) - \boldsymbol{\theta}(\boldsymbol{s}_i)$$

where $\hat{\boldsymbol{\theta}}(\boldsymbol{s}_i)$ is the vector of AOA measurements for emitter i and $\boldsymbol{\theta}(\boldsymbol{s}_i)$ has the exact AOAs for an emitter at $\boldsymbol{s}_i$:

$$\hat{\boldsymbol{\theta}}(\boldsymbol{s}_i) = \begin{bmatrix} \hat{\theta}_{i1} \\ \vdots \\ \hat{\theta}_{i,K_{\rm A}(i)} \end{bmatrix}, \quad \boldsymbol{\theta}(\boldsymbol{s}_i) = \begin{bmatrix} \angle \boldsymbol{d}^{\rm A}_{i1} \\ \vdots \\ \angle \boldsymbol{d}^{\rm A}_{i,K_{\rm A}(i)} \end{bmatrix}.$$

Finally the TDOA cost function is

$$J_{\rm TD}(\boldsymbol{s}_i) = \boldsymbol{e}_{\rm TD}^T(\boldsymbol{s}_i)\boldsymbol{\Sigma}_{\rm TD}^{-1}(i)\boldsymbol{e}_{\rm TD}(\boldsymbol{s}_i),$$
$$\boldsymbol{e}_{\rm TD}(\boldsymbol{s}_i) = \hat{\boldsymbol{g}}(\boldsymbol{s}_i) - \boldsymbol{g}(\boldsymbol{s}_i)$$

where $\hat{\boldsymbol{g}}(\boldsymbol{s}_i)$ is the vector of range-difference-of-arrival (RDOA) measurements obtained by multiplying TDOA measurements with speed of propagation (i.e., speed of light), and $\boldsymbol{g}(\boldsymbol{s}_i)$ is the vector of exact RDOAs:

$$\hat{\boldsymbol{g}}(\boldsymbol{s}_i) = \begin{bmatrix} \hat{g}_{12}(\boldsymbol{s}_i) \\ \vdots \\ \hat{g}_{1,K_{\rm TD}(i)}(\boldsymbol{s}_i) \end{bmatrix}, \quad \boldsymbol{g}(\boldsymbol{s}_i) = \begin{bmatrix} \|\boldsymbol{d}^{\rm TD}_{i2}\| - \|\boldsymbol{d}^{\rm TD}_{i1}\| \\ \vdots \\ \|\boldsymbol{d}^{\rm TD}_{i,K_{\rm TD}(i)}\| - \|\boldsymbol{d}^{\rm TD}_{i1}\| \end{bmatrix}.$$

The noise covariance matrices $\boldsymbol{\Sigma}_{\rm X}(i)$ are assumed to be fixed and independent of $\boldsymbol{s}_i$, and are computed using an initial guess for the emitter locations. The hybrid MLE is given by

$$\hat{\boldsymbol{s}}_i = \arg\min_{\boldsymbol{s}_i} J_{\rm MLE}(\boldsymbol{s}_i) \tag{23}$$

which is a nonlinear least-squares estimator. In general the hybrid MLE does not have a closed-form solution. Iterative search algorithms are available to solve (23) numerically.

VI. Simulation Studies

In the first set of simulations we have two emitters and two teams of UAVs each with three UAVs (i.e., $K_1 = K_2 = 3$). There are three ground threats to be avoided by means of soft constraints. Fig. 1 shows the simulated optimal UAV trajectories for different sensor mixes along with stationary emitter and threat locations. In the simulations the threat avoidance parameters are set to $\kappa_1 = \kappa_2 = 500$, $\kappa_3 = 2000$. The effectiveness of collision avoidance is illustrated in Fig. 1(b). The circular-loop UAV trajectories arising from the maximum turn rate and hard constraints are shown in Fig. 1(c). Observe that different sensor combinations have markedly different optimal paths and lead to different angular sensor separations on the circular hard constraint. While equiangular sensor separation is optimal for SC and TDOA sensors (Figs. 1(a) and (d)), for AOA sensors 60° sensor separation is also an optimal configuration as can be seen from Fig. 1(d) [12]. For other sensor combinations shown in Fig. 1(e), heterogeneous sensor placements producing perpendicular bearing lines result in optimal configurations. The simulation parameters are $v = 30$ m/s, $\rho = 20$, $\omega = \pi$ rad/s, $d_1 = 5$ km, $d_2 = 8$ km, $\beta_1 = 5$, $\beta_2 = 8$, $T = 1$ s, $\varphi = 5^\circ$/s, $\gamma = 0.8$, $\Delta = 1$ m, $\sigma_{\rm S} = 10^{-7}$, $\sigma_{\rm A} = 2\pi \times 10^{-5}/180$ and $\sigma_{\rm TD} = 0.0015$.

The final simulations demonstrate joint path optimization and dynamic sensor allocation. Fig. 2 shows the sensor assignment, and the resulting MSE and $A_{1\sigma}$ curves for two UAV teams ($\sigma_{\rm S} = 5 \times 10^{-8}$, $\sigma_{\rm A} = 2\pi \times 10^{-5}/180$, $\sigma_{\rm TD} = 0.0015$). The MSE exhibits jumps during changes from one sensor combination to another even though $A_{1\sigma}$ keeps decreasing. This can be attributed to sudden changes in the major and minor axis of the error ellipse that increase the MSE while decreasing the area of the error ellipse.

VII. Conclusion

We have developed an iterative real-time steering algorithm for geolocation of multiple stationary emitters from UAV teams equipped with heterogeneous sensor mixes. The steering algorithm aims to maximize the Fisher information matrix approximated using available emitter location estimates and is capable of implementing soft/hard constraints imposed by geometric constraints, as well as, intra-team and inter-team collision avoidance. It also lends itself to joint path optimization and dynamic sensor allocation in a straightforward way.

References

[1] H. Hmam, "Scan-based emitter passive localization," *IEEE Trans. on Aerospace and Electronic Systems*, vol. 43, no. 1, January 2007.

[2] K. Doğançay, "Bias compensation for the bearings-only pseudolinear target track estimator," *IEEE Trans. on Signal Processing*, vol. 54, no. 1, pp. 59–68, January 2006.

[3] ——, "Emitter localization using clustering-based bearing association," *IEEE Trans. on Aerospace and Electronic Systems*, vol. 41, no. 2, pp. 525–536, April 2005.

[4] ——, "Passive emitter localization using weighted instrumental variables," *Signal Processing*, vol. 84, no. 3, pp. 487–497, March 2004.

[5] L. Marsh, D. Gossink, S. P. Drake, and G. Calbert, "UAV team formation for emitter geolocation," in *Proc. of Information, Decision and Control Conference, IDC 2007*, Adelaide, Australia, February 2007.

[6] Y. Oshman and P. Davidson, "Optimization of observer trajectories for bearings-only target localization," *IEEE Trans. on Aerospace and Electronic Systems*, vol. 35, no. 3, pp. 892–902, 1999.

[7] V. V. Fedorov, *Theory of Optimal Experiments*. New York: Academic Press, 1972.

[8] G. C. Goodwin and R. L. Payne, *Dynamic System Identification: Experiment Design and Data Analysis*. New York: Academic Press, 1977.

[9] D. Uciński, *Optimal Measurement Methods for Distributed Parameter System Identification*. Boca Radon, Florida: CRC Press, 2005.

[10] K. Doğançay, "Online optimization of receiver trajectories for scan-based emitter localization," *IEEE Trans. on Aerospace and Electronic Systems*, vol. 43, no. 3, pp. 1117–1125, July 2007.

[11] H. Goldstein, *Classical Mechanics*, 2nd ed. Addison-Wesley, 1980.

[12] K. Doğançay and H. Hmam, "Optimal angular sensor separation for AOA localization," *Signal Processing*, vol. 88, no. 5, pp. 1248–1260, May 2008.

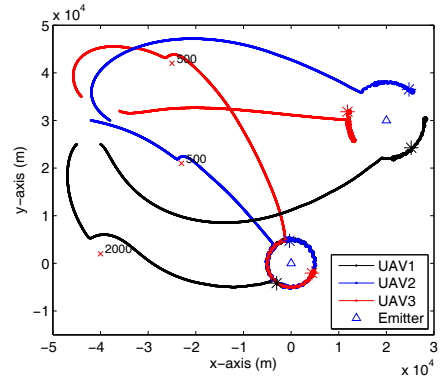

(a)

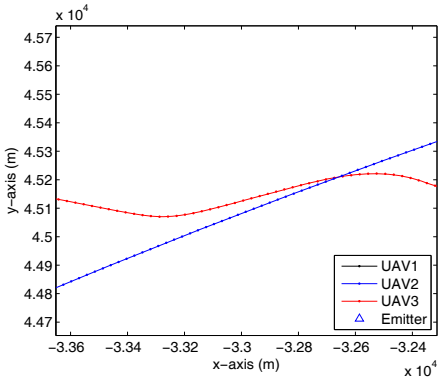

(b)

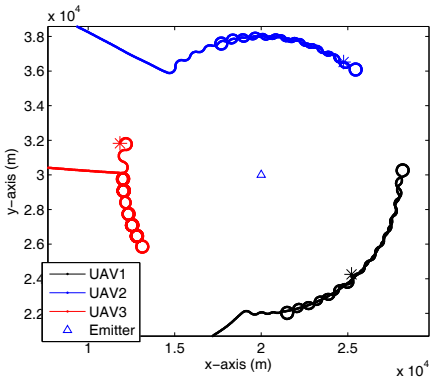

(c)

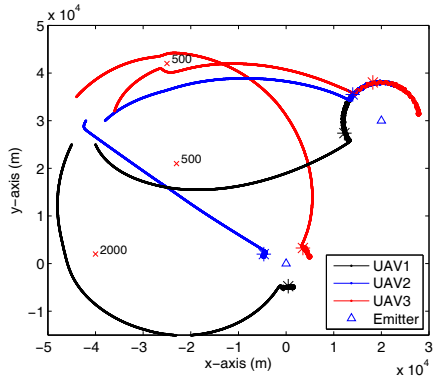

(d)

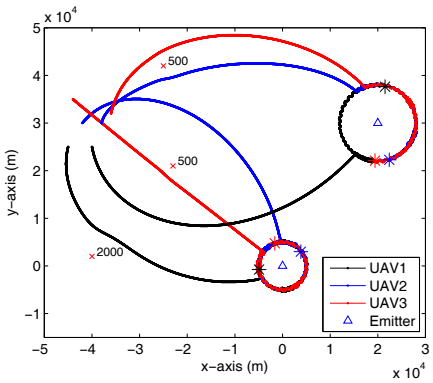

(e)

Fig. 1. Centralized path planning for two UAV teams with final emitter locations marked with "∗" (Team 1 and 2 are assigned to emitters at $\boldsymbol{s}_1 = [0, 0]^T$ and $\boldsymbol{s}_2 = [20, 30]^T$ km, respectively): (a) Team 1 sensors:SC, SC, SC; Team 2 sensors: SC, SC, SC; (b) Close-up of (a) to demonstrate 2D collision avoidance; (c) Team 2 trajectories while circling emitter; (d) Team 1 sensors: TDOA, TDOA, TDOA; Team 2 sensors: AOA, AOA, AOA; (e) Team 1 sensors: SC, SC, AOA; Team 2 sensors: TDOA, TDOA, AOA.

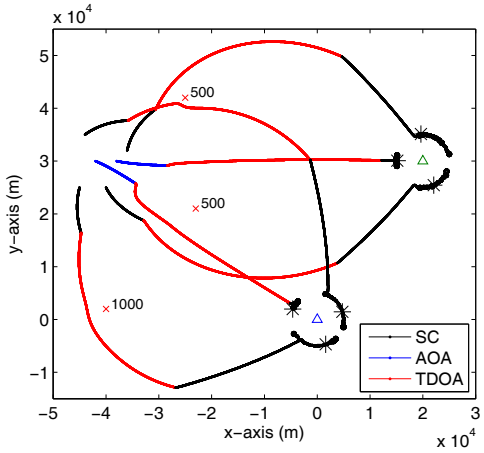

(a)

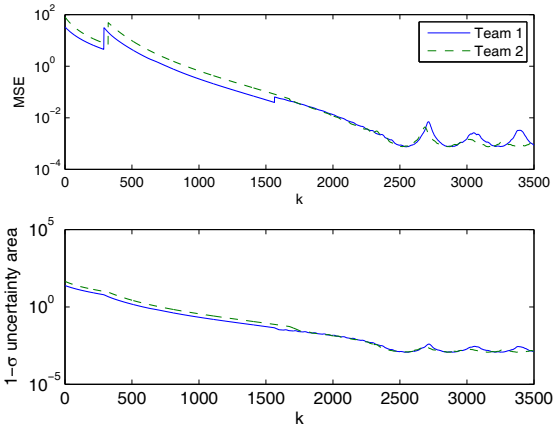

(b)

Fig. 2. Dynamic sensor allocation.